Triaxial Cell for Determining Shielded Cable Transfer Impedance During Environmental Stress

Oskari Leppäaho, Frederic Lafon, Priscila Fernandez-Lopez, Marine Stojanovic, Tim Claeys, Richard Perdriau, Mohamed Ramdani

Triaxial Cell for Determining Shielded Cable Transfer Impedance During Environmental Stress

Oskari Leppäaho, *Graduate Student Member, IEEE,* Frédéric Lafon, *Senior Member, IEEE,* Priscila Fernandez-Lopez, Marine Stojanovic, Tim Claeys, *Member, IEEE,* Richard Perdriau, *Senior Member, IEEE,* and Mohamed Ramdani, *Senior Member, IEEE*

***Abstract*—Transfer impedance is a main characteristic to describe the shielding performance of shielded cables at least up to 1 GHz. Traditionally, methods like line-injection and triaxial cell have been used to characterize it at ambient laboratory conditions. While the ambient laboratory conditions might represent appropriate environmental conditions for some industries, in others, like automotive, they are only a small subset of the real conditions. Thus, there is a need to characterize the transfer impedance over different environmental conditions. In this article, the authors present and verify a new triaxial cell design that is aimed to provide reliable measurements during high thermal and mechanical stresses. First, the cell performance is compared to a commercial cell at laboratory ambient conditions. Then, measurements are performed with the new cell at highly accelerated life testing conditions. Under these high thermal and mechanical stress conditions the cell performance is verified, and results on typical shielded cable performance under the same conditions are given.**

***Index Terms*—Electromagnetic compatibility, cable shielding, transfer impedance, aging, reliability.**

I. Introduction

SHIELDED CABLES have been used for data transmission for over a hundred years after Heaviside's first patent of a coaxial cable [1]. While some modern data transmission has shifted to unshielded twisted pairs (UTP) and optical links, a major part of high-speed data transmission still relies on shielded cables.

In automotive, the future trends of electrification and advanced driver-assistance systems (ADAS) still rely heavily on the use of shielded cables in one form or other: shielded twisted pairs, twinaxial (an impedance controlled non-twisted shielded pair) or traditional coaxial cables for data [2] and shielded power cables for electrification.

In aerospace, data transmission is moving towards fiber optics [3], but electrification keeps shielded cables on the agenda. Especially, shielding the new medium-voltage power distribution systems remains a concern [4].

Manuscript received on May 16, 2022, revised on August 29, 2022 and November 25, 2022, accepted on February 4, 2023.

O. Leppäaho, F. Lafon, P. Fernandez-Lopez, and M. Stojanovic were with Valeo, 94000 Créteil, France. T. Claeys was with KU Leuven, 8200 Bruges, Belgium. R. Perdriau, and M. Ramdani were with ESEO, 49100 Angers, France. O. Leppäaho, R. Perdriau, and M. Ramdani were also with IETR, 35000 Rennes, France.

The research leading to these results has received funding from the European Union's Horizon 2020 research and innovation programme under the Marie Skłodowska-Curie grant agreement No 812.790 (MSCA-ETN PETER). This publication reflects only the authors' view, exempting the European Union from any liability. Project website: http://etn-peter.eu/.

In the manufacturing industry, the fourth industrial revolution is increasing data usage that drives communication needs. Some of those communication links will be wireless, some optical, but some part will remain in shielded cables. Similarly to mobility industry, the advent of power electronics is constantly increasing the amount of variable frequency drives that will have applications that need shielded cables for EM disturbance [5] and bearing current control [6].

With the aforementioned advent of the increased electrification on many industries, it has become more crucial to characterize the performance of shielded cables over their lifetime to ensure that systems using them remain reliable. One important performance parameter of a shielded cable is its transfer impedance [7]. Transfer impedance of typical shielded cables can be defined per unit-length as

$$z_T = r_T + j\omega l_T \tag{1}$$

consisting of transfer resistance r_T and transfer inductance l_T, where both r_T and l_T are complex, frequency dependent variables due to skin-effect. This model covers all the cables studied in this paper. For solid shields, only r_T is relevant [8], and $l_T = 0$. In case they have openings, l_T is not zero, and depends on the shape and amount of the openings [9]. For helical shields, as most foil shields are wound, r_T and l_T are derived from solid shield's r_T and its internal impedance with some helix specific coefficients applied to them [9]. For braided shields, both terms can be defined for a single braid [10] or a combination of two braids [11]. A theory to combine arbitrary shield configurations is also available [9]. Often, accurate definitions add unnecessary complexity, and both r_T and l_T are commonly treated as frequency independent real values without significant loss of accuracy [7]. However, this approach is not valid for shields with low l_T as skin-effect reduces r_T before the inductive impedance is large enough to compensate for it.

Many methods have been used to characterize transfer impedance along the years, the most important ones being line-injection [12], triaxial [13], and reverberation chamber [14] methods. A fairly recent listing of other methods can be found in [15]. While it has been shown that the line-injection method has the widest frequency range starting from DC [16], the triaxial method has been a go-to method for many practitioners due to its robustness and homogeneous field excitation. The aforementioned methods have been complemented by the reverberation chamber method that is valid from a few hundred of megahertz to at least 10 GHz.

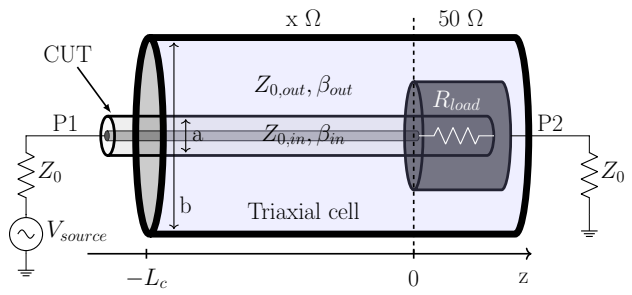

Fig. 1. Overview of the triaxial measurement principle

The effect of environmental stresses to shielded cables has been studied on the level of dielectrics to understand the dependency of RF losses [17] and dielectric strength on temperature [18], and other stresses like radiation [19]. Now, the authors extend these studies to evaluate the dependency of shielded cable transfer impedance on thermal and vibration stresses.

In this paper, the authors present a new triaxial cell design intended for environmental testing of shielding effectiveness (SE) and transfer impedance of shielded cables. The cell design is discussed in Section II. A comparison of RF performance against a commercial cell in laboratory ambient conditions is drawn in Section III, and in Section IV the cell design is verified during highly accelerated life tests (HALT) [20]. Section IV presents typical transfer impedance responses of shielded cables to steady-state and cyclic thermal stress, random vibration, as well as combined cyclic thermal stress and random vibration. Finally, aging is evaluated by comparing measurement results of fresh samples to the ones that have undergone the environmental test cycle.

II. Triaxial Cell

Different configurations of the triaxial cell for measurement of shielded cable transfer impedance have been analyzed [13], and some of them are standardized [21]. An overview of the measurement principle is given in Fig. 1, where a transmission S-parameter S_{21} is measured between P1 and P2. Measurements can be done either by using a combination of a signal generator and a spectrum analyzer, or with a vector network analyzer (VNA). In the measurements of this paper, a VNA is exclusively used.

Transfer impedance can be derived from measured S_{21}, length L_c, and termination R_{load} of the cable-under-test (CUT) [21]

$$z_T = \frac{R_{load} + Z_0}{2L_c} S_{21}, \tag{2}$$

where Z_0 is the impedance of the VNA. This corresponds to the short-circuited near-end configuration assuming high optical coverage of the shields and electrically short L_c, so that transfer admittance y_T and propagation effects can be omitted.

The design of the environmental triaxial cell is shown in Fig. 2. The main characteristics of the cell are gathered in Table I. The given transfer impedance measurement frequency range can be extended to cover the full shielding effectiveness frequency range by extrapolating through the first resonance points due to the sample length [22].

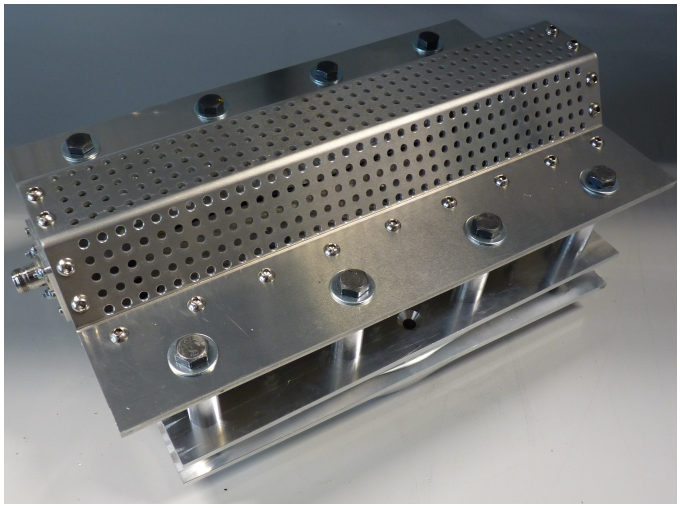

(a)

(b)

Fig. 2. Triaxial cell overview as (a) fully assembled and (b) cover removed

TABLE I
Triaxial Cell Characteristics

Parameter	Symbol	Value
Major diameter	b	90 mm
Sample length	L_c	25 cm
Cell length	-	40 cm
Temperature range	-	-50°C – 120°C
Vibration range	-	0 – 80g_{rms}
Frequency range for shielding effectiveness	-	0 – 1 GHz
Frequency range for transfer impedance	-	0 – 30 MHz

The cell was constructed from 3 mm thick aluminum sheet metal with 15 mm thick end terminations. Its nominal internal diameter was set to 90 mm. That is the same as the one of a commercial cell available to the authors. Thus, it enabled direct comparisons at laboratory ambient conditions. The diameter selection is not critical to measurement results, as the measured transfer impedance has been shown to be independent of the triaxial cell diameter, as long as the TEM-wave condition is sustained [23]. Critical design choices are discussed in Sections II-A and II-B, where the cell body and CUT termination design are respectively addressed.

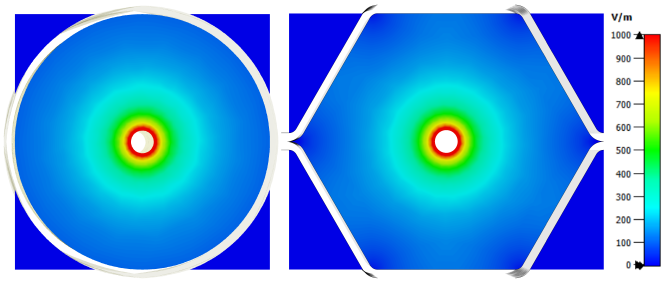

Fig. 3. E-field strength at circular and hexagonal cross-sections of the triaxial cell at 1 GHz

A. Hexagonal cross-section and perforations

To enable fast CUT change, the triaxial cell was designed to be split into two halves. For light weight, the cell design was based on an aluminum sheet metal structure. After iterations, the traditional round design was substituted with a hexagonal design to ease the manufacturing.

The most important features of the overall cell design are:

1) Stable characteristic impedance
2) Uniform field around the cable sample

To assess these features of the hexagonal design, a 3D FEM-simulation was carried out. There, the hexagonal design was compared to a round one, and E-field results at 1 GHz are reported in Fig. 3. As the simulation result ended up with only the TEM-mode present up to the maximum frequency of 3 GHz, the H-field magnitude can be calculated from the presented results with the help of the free-space wave impedance [24]. The field distribution and strength close to the cable sample are equal with both cross-sections. The hexagonal cross-section shows some different field strength pattern close to its boundaries. It means that the free air-space between the CUT and the cell wall should be larger than the cable diameter for all CUTs. This condition is satisfied for all the samples that the authors plan to test in this cell.

Following the successful cross-section change, the next challenge authors wanted to address was to improve the airflow in the triaxial cell. A traditional closed cell will trap air inside acting as a good insulator during thermal tests. Thus, most of the heat would be conducted to the sample through its mounting at the terminations. However, one of the terminations connects the cable shield just to the center pin of the N-connector as plastic mounting hardware and dielectric insulate the termination structure limiting any thermal conduction to the cable. This is a very ineffective way of thermal energy transfer resulting in long time constants to reach thermal equilibrium.

To improve thermal transfer by introducing proper airflow around the CUT, a 10-by-10 mm grid of 5 mm holes was drilled on the covers of the hexagonal cell as can be seen in Fig. 2. The effect of this perforation was also studied with 3D FEM-simulation. The results on E-field strength at 1 GHz across the cell in Fig. 4 show that the perforations have minimal effect on the field distribution inside the cell, and thus, to the characteristic impedance of the cell. Only a small difference is seen close to the cell wall, where

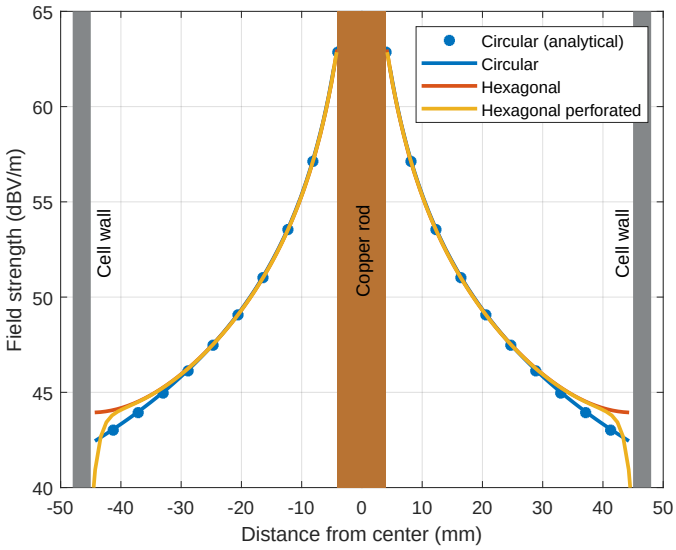

Fig. 4. E-field strength at cross-sections of different cell designs at 1 GHz

the E-field magnitude decreases earlier than with the solid designs. However, it will not have a practical effect on the measurements performed. Again, the H-field results follow the E-field as indicated above. The reference field strength for the circular design was analytically calculated as shown in the Appendix following an approach given in [24] to confirm the accuracy of the simulations.

B. Terminations and ferrules

The second topic in the cell design deserving special attention is the cable shield mounting into the body of the triaxial cell. The quality of this joint is assessed by looking at three design parameters:

1) Stable and low contact resistance
2) Mechanically robust structure
3) Ease of changing the sample

A stable and low contact resistance is paramount at the end where the CUT is fed as, at that end, the termination makes a short-circuit between the cable shield and the triaxial cell body. Any resistance of that contact will be seen as the resistance of the braid, and thus, as error in the measured transfer resistance. Mechanically robust structure is needed, not only to ensure the stability of the contact resistance during environmental stress, but also to withstand all the stresses that the hanging cable will exert to the terminations during vibration testing. Last, test time at environmental testing laboratories is generally expensive. In order to exploit it the best way possible, the CUT sample should be easy and fast to change.

Against these requirements, four termination methods are graded in Table II:

1) Soldering the cable shield is a robust method, but it is difficult to make and disassemble when used with parts that have large thermal masses, like the termination plates in Fig. 5.
2) BNC-connector or similar quick-connect type would provide very fast sample change possibility, but would

TABLE II
COMPARISON OF THE CABLE SHIELD TERMINATION METHODS

Characteristic	Soldering	Connector	Pressure	Ferrule
Initial contact resistance	+ + +	- -	-	+ +
Contact resistance stability	+ + +	- - -	-	+ +
Mechanical robustness	+ +	+	+ +	+ + +
Ease of sample change	- - -	+ + +	+ +	+

+ + + Excellent, + + Very Good, + Good, - Fair, - - Poor, - - - Bad

TABLE III
MEASURED CONTACT RESISTANCES

Contact	Resistance-to-Connector
Short-circuit termination	185 $\mu\Omega$
N-center-pin termination	1.87 $m\Omega$

lack robustness. An N-connector could fare better, but would still not reach the quality of the solder joint.

3) Pressure contact can be made with pressure plates like in the commercial cell that is used as a reference in this paper.
4) Ferrule method uses widely available hydraulic fittings to connect the cable shield to the triaxial cell. Cable shield is crimped and soldered into a specifically designed ferrule that is then joined to the hydraulic fitting.

Grading was made by the authors to help in the selection of the best termination, but it is not intended to be an absolute reference. Based on it, the ferrule termination method was selected. Fig. 5a shows the exploded view drawing of the short-circuited termination. Fig. 5b shows the floating termination, where a similar structure is used with the exception that the adapter is now replaced with a blind termination that is supported with a high-temperature (HT) plastic isolating it from the termination plate. Note, that the thin copper rod is subject to vibration stress, and for the sake of longevity of the test setup, a small part of it should be replaced with a braid to provide sufficient stress relief.

Measured contact resistances of both termination assemblies in Fig. 5 are gathered in Table III. They were measured from the ferrule to the N-connector body for short-circuited termination, and from the ferrule to the center pin of the N-connector for the floating termination. The measurements were done with a BK Precision 2841 DC resistance meter. The values achieved correspond to very good contact performance and enable reliable operation of the test system.

III. RF TESTING

Initial testing of the developed triaxial cell was performed at ambient laboratory conditions. There, two important facets of the cell operation were tested. The cell performance with a copper pipe calibration piece is discussed in Section III-A. The copper pipe is of the same diameter as the rod used in the simulation studies in Section II-A. In Section III-B, the cell performance in transfer impedance measurement of a typical braided cable is discussed. The test results are compared to the ones of a commercial circular triaxial cell in both sections.

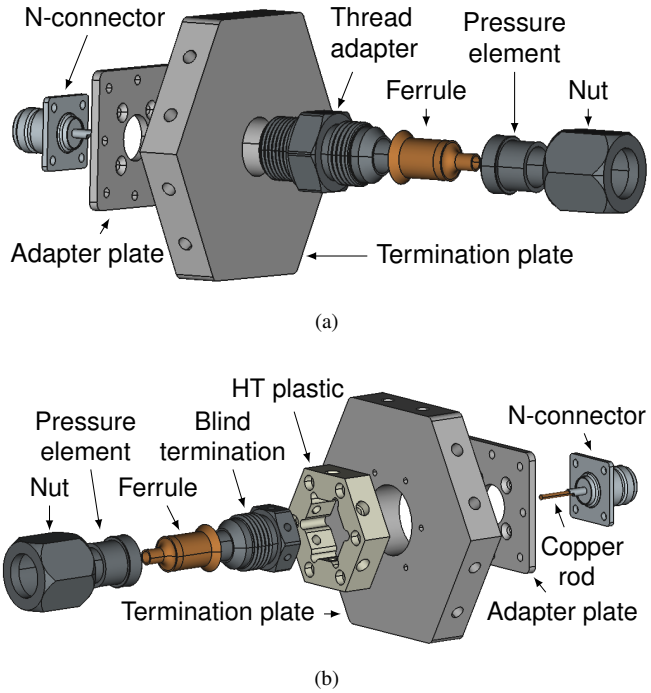

Fig. 5. Exploded view drawings of the (a) short-circuited termination and (b) floating termination

A. Cell Results

The reflection coefficient measurement of the outer cell is shown in Fig. 6. From the magnitude measurement comparison it can be seen that there is no excess attenuation or radiation from the hexagonal perforated cell below 1 GHz, but the magnitude starts to deteriorate above it. In fact, the performance is even better than that of the commercial cell up to 1 GHz. After 1 GHz, the phase angle does not show strong resonances in the cell, but instead changes slowly as a function of frequency with only minor resonances indicated at multiples of the first resonance frequency. It indicates that after 1 GHz there are frequencies, where either most of the incident power actually reflects from an impedance discontinuity between the copper rod and the blind termination shown in Fig. 5b or radiates from the perforation structure. The differences seen on the reflection coefficient phase between the commercial and perforated hexagonal cells below 1 GHz are due to slightly different length of the cells, and are thus expected.

As a conclusion, the perforated hexagonal cell design of this paper works comparably to the reference commercial cell up to 1 GHz. At higher frequencies, the perforated hexagonal cell does not illuminate the CUT correctly either due to the termination design or the perforations as explained in the previous paragraph. The commercial cell offers adequate performance up to 3 GHz, where the measurement range ended.

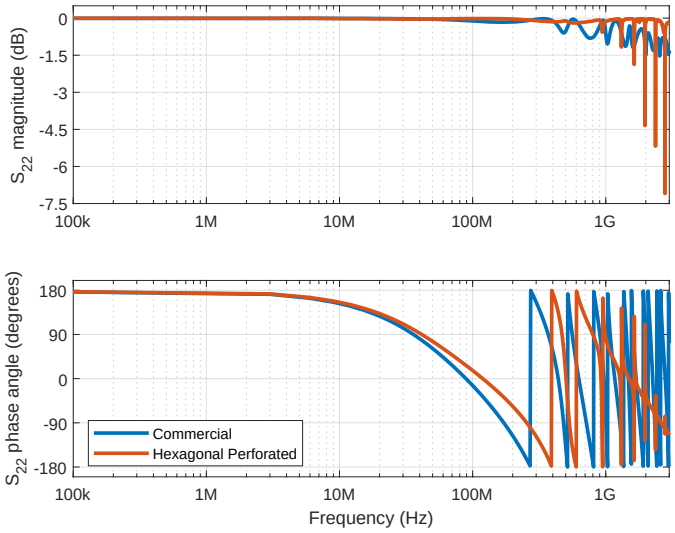

Fig. 6. Reflection coefficient of the outer circuit (P2 in Fig. 1) with an 8-mm copper pipe

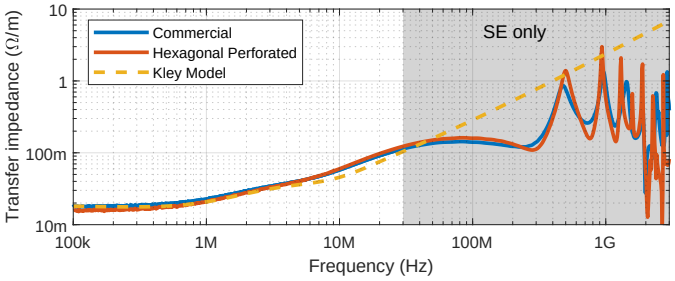

Fig. 7. Transfer impedance measurement comparison with an RG-58C/U

B. Cable Results

The transfer impedance measurements of a generic RG-58C/U-cable are shown in Fig. 7. Below 1 MHz, the commercial cell shows a higher measurement value. This is mainly due to the pressure clamp contacts employed in it to interface with the cable shield. These clamps do not always fit perfectly, and can exhibit an increased contact resistance. From 1 MHz to 100 MHz the fit is excellent between the two cells. At higher frequencies there are some discrepancies, where first the perforated hexagonal cell seems to perform better with the resonance peaks at the transfer inductance envelope up to 1 GHz. The resonance points between the two measurements are very close to each other as the measured cable length was very similar: 30 cm for the commercial, and 25 cm for the perforated hexagonal cell. Afterwards, the findings of Section III-A are confirmed as the measurement result of the perforated cell starts to suddenly drop likely due to the weakened illumination. The results match well with the state-of-the-art model [10].

As a conclusion, both cells are capable of measuring the transfer impedance up to 30 MHz without resonances, and the perforated hexagonal cell seems to follow the envelope of the increasing transfer impedance better up to 1 GHz. Neither one of the cells seems to provide any reliable transfer impedance measurement above 1 GHz.

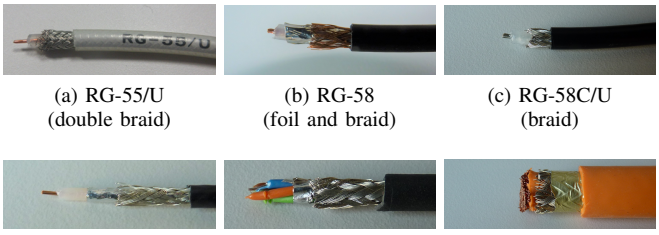

(a) RG-55/U (double braid) (b) RG-58 (foil and braid) (c) RG-58C/U (braid)

(d) Coaxial (foil and braid) (e) LVDS (foil and braid) (f) High voltage (braid and foil)

Fig. 8. Overview of the evaluated cables

TABLE IV
EXTRACTION FREQUENCIES FOR TRANSFER IMPEDANCE ENVIRONMENTAL DEPENDENCY

Cable	f for r_T extraction	f for l_T extraction
RG-55/U	50 kHz	30 MHz
RG-58	10 kHz	500 MHz
RG-58C/U	50 kHz	10 MHz
Coaxial	300 kHz	960 MHz
LVDS	300 kHz	930 MHz
High voltage	300 kHz	10 MHz

IV. Environmental Testing

Environmental testing applied in the scope of this paper is HALT [25]. In the field of mechanical reliability, it has controversial nature as the test chambers are generally not designed for absolute repeatability of the tests, but more to provide extreme test conditions and to withstand them. As a consequence, large uncertainty between the set and measured values as well as thermal gradients need to be tolerated. This means that absolute testing is better done with other methods [20], but for the purposes of this paper the HALT method provides great value for rapid assessment on the feasibility of the developed triaxial cell in environmental testing. Moreover, it can be used to do comparative tests between different technological solutions, like different cable shielding structures. Pictures of the evaluated cables are presented in Fig. 8 with their shield construction highlighted in the captions. The type markings for cables (d) to (f) have been replaced with generic terms due to confidentiality reasons. For each cable, the analysis of environmental dependency is evaluated at two distinct frequencies on the transfer impedance curve so that the first one represents an area, where transfer resistance dominates, and the second one an area, where transfer inductance dominates. The selected frequencies per cable are shown in Table IV. For three cables, transfer inductance needed to be extracted from the shielding effectiveness region as discussed in Section III-B. The first anti-resonance point was used for RG-58, and the second anti-resonance point was used for coaxial and LVDS cables.

The triaxial cell installed in a HALT chamber is shown in Fig. 9. The chamber was setup to run a test cycle that consisted of four distinct phases as shown in Fig. 10:

A) Temperature steps from ambient temperature to -50°C,

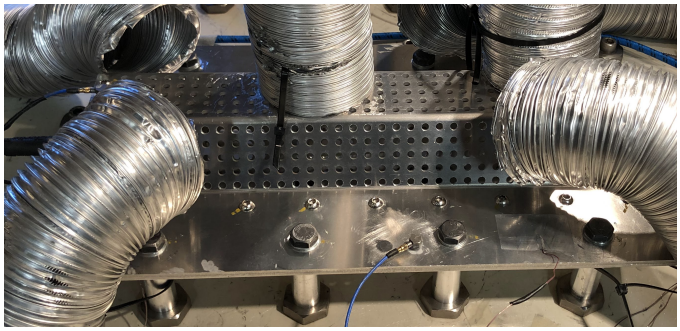

Fig. 9. Triaxial cell in the HALT chamber

and then to 120°C, or to the minimum and maximum tolerable temperature of the CUT according to its datasheet, whichever was more limiting, and no vibration

B) Five cycles between the temperature extremes used in the previous phase with a 5-minute dwell-time at each extreme, and no vibration

C) Increasing vibration level with a $10g_{rms}$ step up to $80g_{rms}$ with a 5-minute dwell-time at each level, and at ambient temperature

D) B and C phases combined with a 10-minute dwell-time per vibration level, and a 5-minute dwell-time per temperature level

Generally, the cable jacket temperature followed the set temperature according to a first order thermal equivalent circuit [26] with a 1-minute time constant, whereas the triaxial cell temperature followed the set-temperature similarly with a 3-minute time constant. Such systems are considered to have reached a steady state after five time constants [27]. This means that the cable jacket reached thermal equilibrium during cyclic testing, whereas the triaxial cell did not. The exact vibration energy transmission to the cable was too challenging to determine reliably, and thus, it is only assumed that the 25 cm mounting span of the cable in the triaxial cell is representative of a typical use case, like vehicle mounting. A more thorough analysis of the achieved temperatures and vibration levels is given in [28].

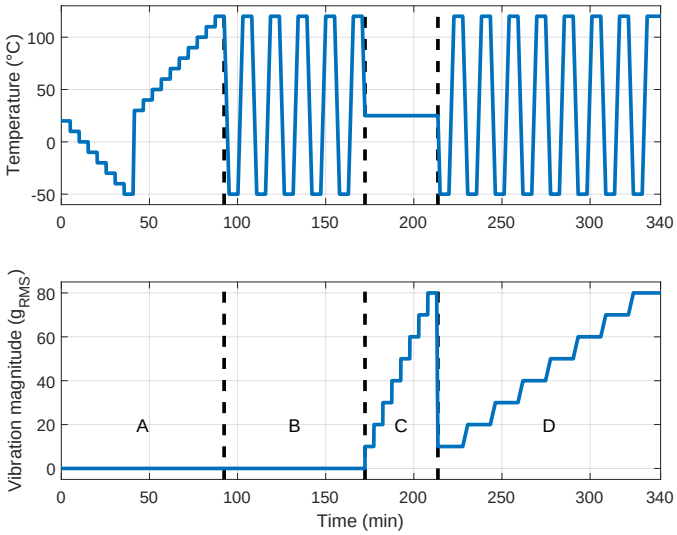

Fig. 10. HALT cycle temperature and vibration set-points

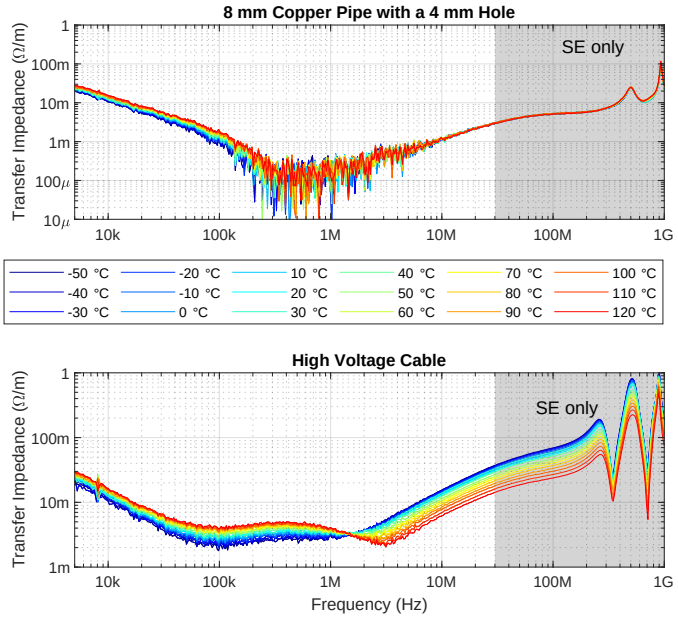

Fig. 11. Temperature dependency of transfer impedance measured during phase A

A. Thermal Tests

Representative results from thermal step tests are shown in Fig. 11. The upper plot shows the transfer impedance of a copper pipe with a 4 mm hole drilled on the side of the pipe to introduce a small constant transfer inductance. Otherwise, it is similar construction as introduced in Section III.

Below 100 kHz, the transfer impedance curves vary proportionally to $1/f$. This is not due to the CUT nor the triaxial cell, but due to a well-known return-current division [13] that depends on the transfer resistance of the test cables, and on the loop inductance of the whole measurement setup. As both measurement ports (P1 & P2) are connected to the same ground reference at VNA, return current is divided between the test cable shields proportionally to their resistance at low frequencies causing an erroneous measurement result. As the frequency increases, the increasing loop impedance forces the return current to follow the smallest loop i.e. the shield of the injecting cable. This effect could be minimized by using shorter test cables with better transfer resistance characteristics, or by adding ferrites on top of the test cables to increase loop inductance. Unfortunately, none of these methods were available to the authors during HALT testing. Between 100 kHz and 10 MHz, the VNA dynamic range limited the measurement accuracy. Above 10 MHz no change in the measurement result is seen for the 8 mm copper pipe with a 4 mm hole. It means that the triaxial cell does not show temperature dependency on its measurement result. A representative transfer impedance thermal dependency graph is given in the bottom part of Fig. 11 for the high voltage cable.

Further results for the evaluated cables are given in Table V. There, linear regression with least squares approach

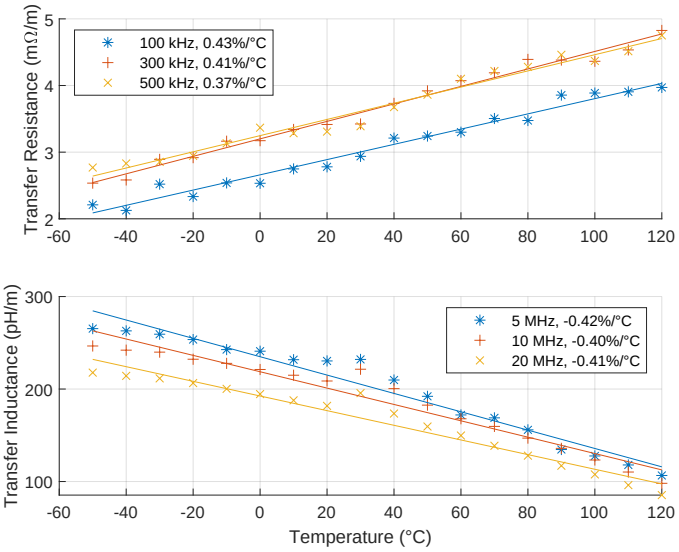

Fig. 12. Temperature dependency of transfer resistance and inductance of a high voltage cable

was used to arrive at the temperature coefficients that can be used as a simple model. These coefficients were then normalized to enable comparison between different cables with different magnitudes of transfer resistance and inductance. The extracted coefficients were sufficiently stable over different frequencies as demonstrated in Fig. 12.

Transfer resistance thermal dependency was generally between that of a copper ($0.40\%/°\mathrm{C}$) and an eutectic SnPb alloy ($1.0\%/°\mathrm{C}$) [29]. The results were within this interval for all the other samples except the coaxial sample. Its variation could be explained by e.g. NiCr ($0.008\%/°\mathrm{C}$) [30] impurities in the braiding causing reduced thermal dependency.

Transfer inductance thermal dependency from cable to cable was less uniform with both positive and negative temperature coefficients. To consider thermal expansion of materials as an explanation for the transfer inductance change, Kley-model [10] was used to calculate the difference in transfer inductance as the braid diameter varied. As the Kley-model is for single-braided cables, RG-58C/U cable was selected as an example. Its dielectric consists of polyethylene [31], which has a worst-case linear thermal expansion coefficient of $3.5 \cdot 10^{-4}°\mathrm{C}^{-1}$ [32] for the low-density variant. With this value, Kley-model gives an average transfer inductance decrease of $0.15\%/°\mathrm{C}$. Thus, thermal expansion of the dielectric seems to explain approximately one-half of the observed transfer inductance decrease as a function of temperature. A further study will be needed to tie the transfer inductance better into the physical behavior of the cable.

With regards to the cell performance during rapid thermal cycling (phase B in Fig. 10), Fig. 13 shows identical data to Fig. 11, but just at the extreme temperatures. It must be noted that during cycling in phase B, temperature control has a larger error than in phase A. Generally, a $\pm 5°C$ error is expected. All the dependencies were linear, and thus, any value that is lower in the cyclic columns of Table V than the one in the temperature dependency columns is considered to

TABLE V
TRANSFER IMPEDANCE THERMAL DEPENDENCY (TEST PHASES A AND B)

Cable	R_T (%/°C)	L_T (%/°C)	R_T (%/cycle)		L_T (%/cycle)	
			T_{min}	T_{max}	T_{min}	T_{max}
RG-55/U	0.44	0.11	-0.2	-0.5	3.3	1.1
RG-58	0.58	0.79	0.3	0.0	-10	-8.1
RG-58C/U	0.48	-0.28	-0.1	0.1	-0.4	0.5
Coaxial	0.32	-0.48	-0.2	0.2	4.7	2.9
LVDS	0.42	-0.81	0.3	0.0	-4.9	-5.5
High voltage	0.41	-0.40	1.0	0.9	-2.7	-3.6

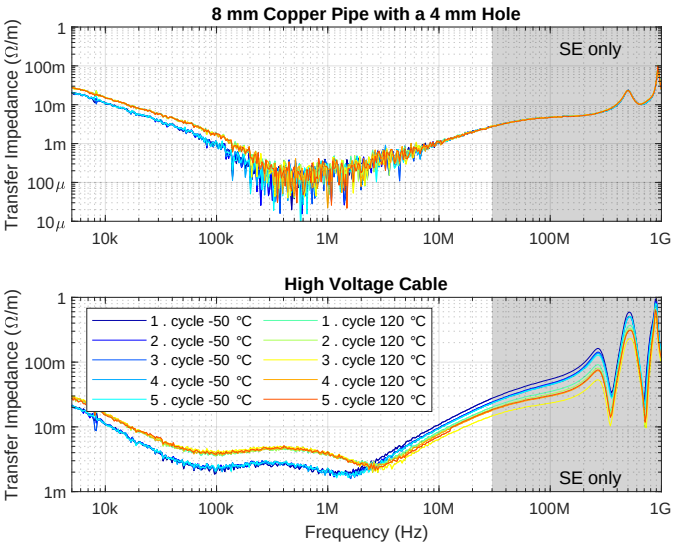

Fig. 13. Transfer impedance over rapid thermal cycles of phase B

present no cyclic dependency. It can be concluded that cyclic thermal stress does not have an effect on the transfer resistance of shielded cables with a small uncertainty on the high voltage cable that showed slightly larger cyclic dependency than expected. However, it has also the largest thermal mass, which could have affected the measured results. From transfer inductance point of view it is evident that thermal cycling will have an effect on it with the exception of cables whose shields consist of braid only. The reason for the inductance change could be the movement of the foil shield, but it has not been studied in this work.

B. Vibration Tests

Representative transfer impedance results from random vibration tests are shown in Fig. 14. Here, the cell verification was done with an RG-58C/U cable as the inner conductor in the copper pipe moved relative to the drilled hole during vibration making the cell validation impossible. It is seen that the triaxial cell does not have an effect on the transfer impedance measurement result within the random vibration range used. Here, the representative cable sample was also changed to the coaxial one that reacted more visibly to vibration.

Linear least squares fitted coefficients for transfer impedance vibration dependency modeling are gathered in

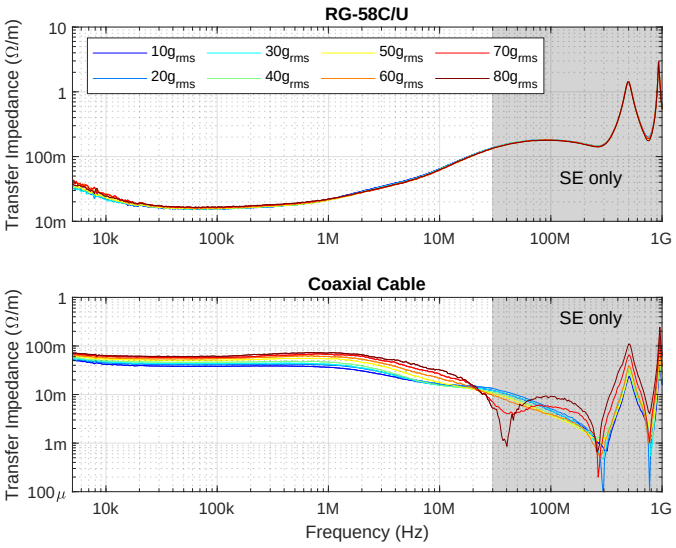

Fig. 14. Vibration dependency of transfer impedance measured during phase C

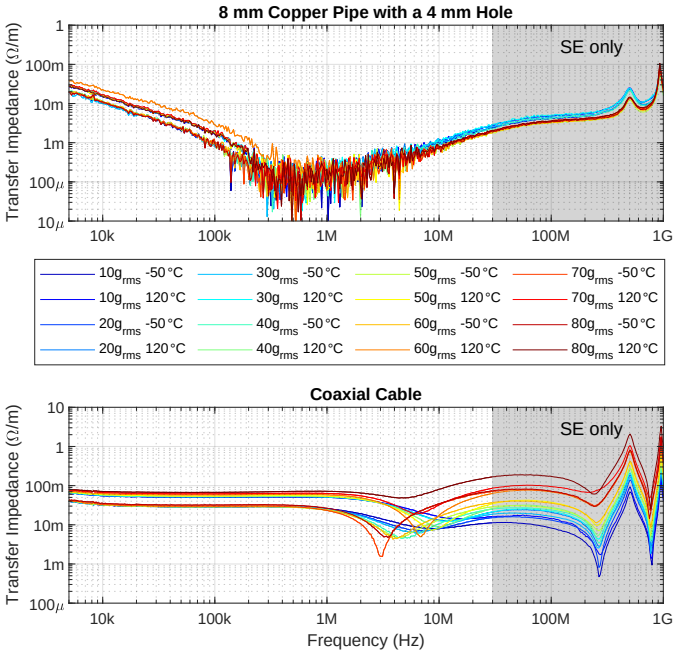

Fig. 15. Transfer impedance dependency on combined vibration and thermal cycling measured during phase D.

TABLE VI
TRANSFER IMPEDANCE VIBRATION DEPENDENCY (TEST PHASE C)

Cable	R_T $(\%/g_{rms})$	L_T $(\%/g_{rms})$
RG-55/U	-0.01	0.61
RG-58	0.00	exp.
RG-58C/U	0.11	-0.06
Coaxial	1.31	exp.
LVDS	0.12	8.51
High voltage	-0.06	0.19

Table VI for all the evaluated cables. It is found out that only the transfer resistance of the coaxial cable has significant linear dependency on vibration amplitude. Transfer inductance wise, the regression results are more divided with some cables, like the RG-58C/U, demonstrating practically no linear or other dependency to vibration, to other cables like the coaxial cable demonstrating exponential dependency. The exponential dependency means in practice that the shield has failed during the test in one way or another. The aging results shown in Section IV-D are likely to explain the reason for the exponential dependency of the transfer inductance.

C. Combined Tests

Representative results from combined vibration and thermal cycling tests are shown in Fig. 15. The thermal transient extremes for the coaxial cable were reduced to -40°C and 105°C due to its ratings. The copper pipe with a 4 mm hole was used again as a reference sample. As the center conductor was not completely fixed, transfer inductance showed some dependency on vibration. However, the measurement results also show the immense stress that this last test step causes to the triaxial cell assembly. At frequencies lower than 100 kHz, several test points show an increased measurement result. Those increased measurement results indicate a loosened test cable at either of the N-connectors. That slight change was the first sign of an imminent cable detachment. Thus, during these tests, the setup needed to be repaired several times.

TABLE VII
TRANSFER IMPEDANCE COMBINED THERMAL CYCLE AND RANDOM VIBRATION DEPENDENCY (TEST PHASE D)

Cable	R_T $(\%/\mathrm{g_{rms}})$		L_T $(\%/\mathrm{g_{rms}})$	
	T_{min}	T_{max}	T_{min}	T_{max}
RG-55/U	0.03	0.01	0.00	0.06
RG-58	0.03	exp.	1.19	exp.
RG-58C/U	0.04	0.02	0.04	0.17
Coaxial	0.11	exp.	9.65	exp.
LVDS	0.01	0.05	20.10	52.90
High voltage	0.07	0.12	-0.18	-0.28

The coefficients for linear least squares fits of combined transfer impedance vibration and thermal dependency are gathered in Table VII for all the evaluated cables. They are formatted as vibration dependencies at T_{min} and T_{max} temperatures. Again, the cables with braided shields seem to be fairly immune to the combined stress, whereas the same cables as in pure vibration tests show exponential dependency on both their transfer resistance and transfer inductance. Interestingly, at low temperatures, the dependency is closer to linear than exponential. This could be linked to the fact that at low temperatures the cable structure contracts being able to hold the shield better in place without space for it to move due to vibration. This effect could be seen to be confirmed by comparing all the transfer inductance results, which show higher linear dependency to vibration at high temperatures.

TABLE VIII
z_T MEASUREMENT RESULTS OF FRESH AND AGED SAMPLES

Cable	r_T (mΩ/m)			l_T (pH/m)		
	Fresh	Aged	Increase	Fresh	Aged	Increase
RG-55/U	7.8	8.0	+3%	7.2	10	1.4×
RG-58	107	112	+5%	4.9	28	4.7×
RG-58C/U	15.6	16.5	+6%	1100	1000	0.9×
Coaxial	44.4	57.5	+30%	21	230	10×
LVDS	20.8	21.7	+4%	2.1	84	40×
High voltage	3.4	3.7	+8%	220	130	0.6×

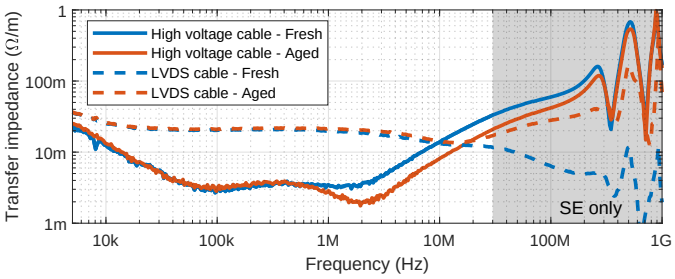

Fig. 16. Fresh and aged transfer impedance measurement comparison

D. Aging During HALT

After HALT tests were finished, cables were cooled down back to the ambient temperature as they were measured at the beginning of the tests. Then, an additional transfer impedance measurement was done to determine if any aging effects could be seen on the shielding performance. The results of these measurements are shown in Table VIII, and they can be directly used to model the cable behavior before and after the test cycle given in Fig. 10. Values in the "Increase"-columns have been calculated before rounding, and might deviate slightly from what can be calculated from the rounded values presented. Transfer impedance graphs for two corner cases: the high voltage cable and the LVDS cable are shown in Fig. 16. They confirm the values reported in Table VIII. No practical difference on transfer resistance between fresh and aged samples is seen, but the transfer inductance for the aged high voltage cable is slightly lower than that of the fresh cable, whereas the shielding effectiveness region result for the LVDS cable shows significantly decreased performance for the aged cable due to increased transfer inductance. Results for the coaxial cable have been previously published in [28].

The r_T increase over the test cycle was within measurement uncertainty except for the coaxial cable. More significant changes were seen in the l_T measurements, where only the RG-58C/U cable can be considered completely immune to the applied aging stress. The LVDS cable with the worst aging result was analyzed after the tests. Fig. 17a shows the cable with jacket removed and Fig. 17b with the braiding removed. It was observed that the braid wires had disorientation due to motion related stress, but they were all intact. The foil shield had teared apart completely close to both mounting points, and had smaller tears along the cable making the foil damage as the most probable cause of the increased l_T.

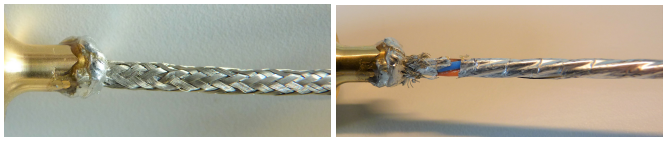

(a) (b)

Fig. 17. LVDS cable with (a) jacket removed and (b) braid removed after the test cycle

V. Conclusion

In this paper, a hexagonal triaxial cell for environmental testing was presented. The design was analyzed with 3D FEM-simulation, and later verified to provide good results compared to a commercial cell at ambient laboratory conditions. Then, it was verified to work well under both thermal stress between -50°C and 120°C, and under random vibration up to $80 g_{rms}$. The temperature swing was mainly limited by the coaxial cables used to connect the triaxial cell to the VNA as they were limited to -55°C and 125°C. The vibration level was close to the maximum of HALT system that was used. Thus, it is possible that the cell design could be used above the aforementioned stress levels.

It was shown that typical shielded cables can have either no dependency on environmental stress, like was the case for RG-58C/U under vibration stress, a limited dependency on the environmental parameter, like for the high voltage CUT under thermal stress, or a high dependency, like for the coaxial CUT during vibration as well as combined vibration and thermal stress. After the tests, some cables, like the RG-58C/U, did not show any signs of aging. On the other hand, some cables with foil shield, like the LVDS cable, showed more than a ten-fold increase in transfer inductance, which was related to tearing of the foil shield.

A logical next step from these results would be to develop better models than the linear ones shown in this paper – possibly taking into account more of the physical cable features. Then, these models could be easily integrated into system simulation to predict product EMC performance during development. This responds to the emerging need to address increasing safety and reliability requirements that modern electronics systems face throughout their lifetime.

Appendix
Triaxial Cell E-field Strength Calculation

The E-field strength

$$E(z,\rho) = -\nabla_t \Phi(z,\rho) \tag{3}$$

is calculated with the help of scalar potential

$$\Phi(z,\rho) = \frac{V(z)\ln\frac{b}{2\rho}}{\ln\frac{b}{a}}, \tag{4}$$

where ρ is the distance from the center of the cell, b is the inner diameter of the triaxial cell, and a is the diameter of the copper rod. To arrive at the correct voltage $V(z)$ along the line, the incident voltage wave amplitude needs to be calculated as

$$V^+ = \frac{V(z)}{\mathrm{e}^{-j\beta z} - \mathrm{e}^{j\beta z}} = \frac{2P_{in}Z_0}{\mathrm{e}^{-j\beta z} - \mathrm{e}^{j\beta z}}, \tag{5}$$

where $z = -385\text{mm}$, input power $P_{in} = 1\text{W}$, and $Z_0 = \sqrt{L/C}$, $\beta = 2\pi f\sqrt{LC}$ are the characteristic impedance and propagation constant of the triaxial cell configuration, respectively. The distributed inductance and capacitance are calculated as

$$L = \frac{\mu_0}{2\pi} \ln \frac{b}{a} \tag{6a}$$

$$C = \frac{2\pi\epsilon_0}{\ln \frac{b}{a}}, \tag{6b}$$

respectively with μ_0 and ϵ_0 as vacuum permeability and permittivity.

Then, the voltage $V(z)$ in (4) can be calculated as

$$V(z) = V^+ \left(\mathrm{e}^{-j\beta z} - \mathrm{e}^{j\beta z}\right), \tag{7}$$

and the field strength in Fig. 4 can be calculated by setting $z = -195\text{mm}$ and sweeping ρ. As seen in Fig. 4, the analytical result matches perfectly with the FEM-simulation result.

ACKNOWLEDGMENT

Authors would like to thank O. Maurice of ARIANE Group for fruitful discussions on shielded cable transfer impedance under environmental stress. Equally, they would like to thank B. Pichereau of Arts et Métiers Angers Campus for providing mechanical design help and improvements, and A. Maire of Valeo Thermal Systems, La Verrière for his excellent design improvement suggestions during initial vibration testing. The authors faced some unexpected failures that could have taken significantly longer to solve without A. Maire pointing out typical fixes for the weak spots found in the design. During HALT, Rohde & Schwartz provided a VNA for the first author to capture the results reported in Section IV.

REFERENCES

[1] O. Heaviside, "Improvements in Electrical Conductors and in the Arrangement and Manner of Using Conductors for Telephonic and Telegraphic Purposes," Great Britain Patent 1407, Oct., 1880.

[2] C. Rusch and B. Bergner, "Robust Connectivity Solutions for Next-Generation Automotive Data Networks," 2019. [Online]. Available: https://www.te.com/content/dam/te-com/documents/automotive/global/robust-connectivity-solutions-wp-en-0819.pdf

[3] H. D. Nguyen, D. H. Ngo, M. Atiquzzaman, J. Sluss, Jr., F. Slaveski, and M. F. Alam, "Fiber-optic communication links suitable for on-board use in modern aircraft," in *Defense and Security*, W. E. Thompson and R. L. Brunson, Eds., Orlando, FL, Sep. 2004, pp. 103–112.

[4] Advanced Research Projects Agency - Energy, "Funding Opportunity Announcement DE-FOA-0001953 - Appendix Q," Nov. 2021.

[5] G. Skibinski, J. Pankau, R. Sladky, and J. Campbell, "Generation, control and regulation of EMI from AC drives," in *IAS 97 Conf Rec 1997 IEEE Ind Appl Conf Thirty-Second IAS Annu Meet*, vol. 2. New Orleans, LA, USA: IEEE, 1997, pp. 1571–1583.

[6] M. Weicker and A. Binder, "Review on system parameters in variable speed AC-induction motor drives with parasitic electric bearing currents," in *2021 23rd Eur Conf Power Electron Appl EPE21 ECCE Eur.*, Ghent, Belgium, 6.

[7] E. Vance, "Shielding effectiveness of braided-wire shields," *IEEE Trans. Electromagn. Compat.*, vol. EMC-17, no. 2, pp. 71–77, May 1975.

[8] S. A. Schelkunoff, "The Electromagnetic Theory of Coaxial Transmission Lines and Cylindrical Shields," *Bell Syst. Tech. J.*, vol. 13, no. 4, pp. 532–579, Oct. 1934.

[9] H. Kaden, "L.3. Kopplungswiderstand von Leitungsschirmen," in *Wirbelströme und Schirmung in der Nachrichtentechnik*. Berlin, Heidelberg: Springer Berlin Heidelberg, 1959, pp. 290–319.

[10] T. Kley, "Optimized single-braided cable shields," *IEEE Trans. Electromagn. Compat.*, vol. 35, no. 1, pp. 1–9, Feb. 1993.

[11] E. F. Vance, "Shielding Effectiveness of Braided Wire Shields," Apr. 1974.

[12] B. Eicher and L. Boillot, "Very Low Frequency To 40 GHz Screening Measurements On Cables And Connectors; Line Injection Method And Mode Stirred Chamber," in *Int. Symp. Electromagn. Compat.* Anaheim, CA, USA: IEEE, 1992, pp. 302–307.

[13] T. Kley, "Measuring the coupling parameters of shielded cables," *IEEE Trans. Electromagn. Compat.*, vol. 35, no. 1, pp. 10–20, Feb. 1993.

[14] B. Démoulin and L. Koné, "Shielded Cable Transfer Impedance Measurements in the Microwave Range of 1 GHz to 10 GHz," *IEEE Electromagn. Compat. Mag.*, no. 229, pp. 52–61, 2011.

[15] P. Deschenes, R. Bijman, and F. Leferink, "Effect of gland quality on the screening effectiveness of cable-connector assemblies," in *2015 IEEE Int. Symp. Electromagn. Compat. EMC*. Dresden, Germany: IEEE, Aug. 2015, pp. 62–67.

[16] B. Démoulin and L. Koné, "Shielded Cable Transfer Impedance Measurements High frequency range 100 MHz–1 GHz," *IEEE Electromagn. Compat. Mag.*, no. 228, pp. 42–50, 2011.

[17] A. J. Bur, "Dielectric properties of polymers at microwave frequencies: A review," *Polymer*, vol. 26, no. 7, pp. 963–977, Jul. 1985.

[18] G. Montanari, G. Mazzanti, and L. Simoni, "Progress in electrothermal life modeling of electrical insulation during the last decades," *IEEE Trans. Dielect. Electr. Insul.*, vol. 9, no. 5, pp. 730–745, Oct. 2002.

[19] S. Nakamura, F. Murabayashi, K. Iida, G. Sawa, and M. Ieda, "Degradation of Dielectric Properties of Polyethylene by Combined Y-Irradiation and Thermal Stresses," *IEEE Trans. Elect. Insul.*, vol. EI-22, no. 6, pp. 715–720, Dec. 1987.

[20] A. Charki, R. Laronde, F. Guérin, D. Bigaud, and F. Coadou, "Robustness evaluation using highly accelerated life testing," *Int J Adv Manuf Technol*, vol. 56, no. 9-12, pp. 1253–1261, Oct. 2011.

[21] IEC 62153-4-3, *Metallic Communication Cable Test Methods – Part 4-3: Electromagnetic Compatibility (EMC) – Surface Transfer Impedance – Triaxial Method*, 2013.

[22] IEC TS 62153-4-1, *Metallic Communication Cable Test Methods – Part 4-1: Electromagnetic Compatibility (EMC) – Introduction to Electromagnetic Screening Measurements*, 2014.

[23] O. Leppäaho, F. Lafon, P. Fernandez-Lopez, M. Stojanovic, R. Perdriau, and M. Ramdani, "Sensitivity of Shielded Cable Transfer Impedance Measurement to Triaxial Cell Diameter," in *2021 Jt. IEEE Int Sym EMCSIPI EMC Eur.*, Raleigh, NC, USA, 2021, pp. 917–921.

[24] D. M. Pozar, "Chapter 2: Transmission Line Theory," in *Microwave Engineering*, 3rd ed. Hoboken, NJ: John Wiley & Sons, Inc., 2005, pp. 49–90.

[25] K. A. Gray and J. J. Paschkewitz, *Next Generation HALT and HASS: Robust Design of Electronics and Systems*, ser. Wiley Series in Quality and Reliability Engineering. New York, NY: John Wiley & Sons, 2016.

[26] P. R. Strickland, "The Thermal Equivalent Circuit of a Transistor," *IBM J. Res. & Dev.*, vol. 3, no. 1, pp. 35–45, Jan. 1959.

[27] N. Storey, "Chapter 9 - Transient Behaviour," in *Electronics: A Systems Approach*, sixth edition ed. Harlow, England London New York Boston San Francisco Toronto: Pearson, 2017, pp. 168–183.

[28] O. Leppaaho, F. Lafon, B. Ferreri, P. Fernandez-Lopez, M. Stojanovic, R. Perdriau, and M. Ramdani, "Including Experimental Aging of Shielded Cables into Bulk Current Injection Simulations," in *2022 Int. Symp. Electromagn. Compat. – EMC Eur.* Gothenburg, Sweden: IEEE, 2022, pp. 811–815.

[29] T. Gancarz, P. Fima, and J. Pstruś, "Thermal Expansion, Electrical Resistivity, and Spreading Area of Sn-Zn-In Alloys," *J. of Materi Eng and Perform*, vol. 23, no. 5, pp. 1524–1529, May 2014.

[30] P. Majumder and A. Bhattacharyya, "A computational study of the impact of the Wiedemann–Franz–Lorenz law on the thermal response of nichrome cylinders," *Modelling Simul. Mater. Sci. Eng.*, vol. 16, no. 1, p. 015006, Jan. 2008.

[31] Nexans, "RG 58 - Coaxial cable with characteristic impedance 50 ohm," Apr. 2010.

[32] eXsource, "Thermal and Electrical Properties of PE." [Online]. Available: http://www.qenos.com/internet/home.nsf/(LUImages)/Tech%20Guide:%20Thermal%20and%20electrical%20properties%20of%20PE/$File/144%20QEN%20eX%20TN%20Thermal%20&%20Electrical%20properties%20of%20PE.pdf

Oskari Leppäaho (GS'20) was born in Seinäjoki, Finland, in 1987. He received the B.Sc.(tech.) and M.Sc.(tech.) degrees in electromagnetics from Tampere University of Technology, Tampere, Finland, in 2014 and 2015, respectively.

From 2013 to 2017, he was with Vacon Oy, Vaasa, Finland. From 2017 to 2019 he was with Danfoss Drives, Loves Park, IL, USA. He is currently working towards a Ph.D. degree at Valeo, Créteil, France and he is affiliated with INSA Rennes, Rennes, France. His current reserach interests include system level modelling, shielded cables and connectors, EMC related grounding structures, and highly accelerated life testing.

Frédéric Lafon (M'14–SM'15) was born in Chennevieres, France in 1974. He received the M.Sc. degree in electromagnetic compatibility (EMC) from the University of Clermont-Ferrand, France, in 2004, the Ph.D. degree in electronics from the Institut National des Sciences Appliquees, Rennes, France, in 2011, and the "Habilitation a Diriger des Recherches" (Accreditation Degree) in Electronics from Universite de Rennes 1, France, in 2016.

In 2000, he joined Valeo, Créteil, France, where he is currently an EMC Master Expert and the Group EMC discipline manager. His current research interests include the characterization and modeling techniques of integrated circuits, for emissions, immunity, and transients (electrostatic discharge), as well as the different techniques to manage EMC at the system level through a bottom-up approach.

Priscila Fernández-López was born in Oviedo, Spain, in 1982. She received the degree in telecommunication engineering from the University of Oviedo, Spain, in 2007 and the Ph.D. degree in electronics from the University of Rouen, France, in 2011.

From 2006 to 2011, she was with Embedded Electronic Systems Research Institute (IRSEEM), Saint-Etienne-du-Rouvray, France. In 2012, she joined Valeo, Créteil, France, where she is an EMC expert at present. Her current research interests include electromagnetic compatibility at integrated circuit and system levels, in particular the integrated circuit characterization and modelling techniques in order to predict the electromagnetic compatibility performance of systems.

Marine Stojanovic was born in Creil, France, in 1992. She received the Engineering degree in electronics and electrotechnics from the Engineering School ESIEE, Amiens, France, in November 2015, the Ph.D. degree in electronics from the Institut National des Sciences Appliquees, Rennes, France, in 2018.

In 2015 she joined Valeo, Créteil, France, where she is currently an EMC Expert. Her current research interests include electromagnetic compatibility, filter design, and EMC simulations.

Tim Claeys (M'20) was born in 1990. He received the M.S. degree in industrial engineering sciences, option electronics, from the University College Katholieke Hogeschool Sint-Lieven Gent, Ghent, Belgium, in 2013, and the Ph.D. degree in electrical engineering from Katholieke Universiteit (KU) Leuven, Leuven, Belgium, in 2018.

Since 2018, he has been a Postdoctoral Researcher with the M-Group Research Group (Lab FMEC), KU Leuven, Bruges, Belgium. His current research interests include near-field scanning, the development of characterization methods for shielding materials and gaskets, electromagnetic interference resilience of wireless protocols, and global reliability of electronic systems.

Dr. Claeys is a member of the IEEE EMC Society Benelux chapter executive committee as the treasurer and communication manager.

Richard Perdriau (M'01–SM'07) was born in Angers, France, in 1971. He received the engineering degree in electronics and computer science from ESEO Angers - Grande Ecole d'Ingénieurs Généralistes, Angers, France, in 1992, the Ph.D. degree in applied sciences from Université Catholique de Louvain, Louvain-la-Neuve, Belgium, in 2004, and the "Habilitation à Diriger des Recherches" (Accreditation Degree) from Université de Rennes 1, Rennes, France, in 2012.

From 1992 to 2012, he was an Associate Professor with ESEO in the fields of microelectronics and embedded systems. In 2013, he became a Full Professor. His research interests include EMC of integrated circuits, mixed-signal hardware description languages, and integrated circuit design.

Dr. Perdriau served as the Vice-Chair and the Technical Program Co-Chair of EMC Europe 2017.

Mohamed Ramdani (M'01–SM'07) was born in Oujda, Morocco. He received the Ph.D. degree in microelectronics from Université Paul Sabatier, Toulouse, France, in 1989, and the "Habilitation à Diriger des Recherches" (Accreditation Degree) from Université de Rennes 1, Rennes, France, in 2004.

From 1991 to 2008, he was an Associate Professor with ESEO, Angers, France, in the fields of microelectronics and microwave electronics. Since 2008, he was a Full Professor. His research interest includes EMC of integrated circuits and integrated circuit design. He has authored several book chapters and many peer-reviewed scientific papers.

Dr. Ramdani was the General Chair of EMC Europe 2017, which was held in Angers, France. He was elected the Vice Chair of the IEEE France Section, in 2016.